Supplementary Material and Methods

Quantification of disc parameters, intensity and mitotic density profiles in discs

Image stacks were projected using a maximum projection and despeckled in ImageJ. Occasionally, when a rat-anti-PH3 antibody had to be used in combination with m-anti-Hairy, there was some bleed-through of PH3 into Hairy. This bleed-through was removed using the outlier tool in ImageJ. Images were then loaded into **matlab** for further analysis.

The position of the furrow and a rectangular region of interest (ROI) were marked on the image by selecting two points on the posterior edge of the Hairy expression domain. The equatorial and polar regions were avoided, because the gradient is compressed or stretched in these regions (Firth et al. 2010) (Fig. 1C). The **furrow position** is the mean column value of positions of the two selected points. (A column on the image corresponds to a position along the anteroposterior axis.)

The values of pixels outside of the disc were set to NaN (not a number), so that they do not contribute to the following analysis.

The **posterior width** is approximately given by the mean number of non-NaN pixels per ROI row posterior to the furrow position times the image spacing (μm/pixel conversion factor). The **anterior width** is determined analogously using the non-NaN pixels located in anterior ROI rows. The **total width** is the sum of the two. The **intensity profiles** of P-Mad and Hairy are given by the mean intensity of the non-

NaN pixels per ROI column. Background was measured and subtracted from the resultant intensity profiles.

The P-Mad **background** was determined as the intensity level at the anterior edge of the disc. This seems to be accurate since in hh^{ts} mutants, after 24h at 29°C, there still is background staining at the edge, of the same intensity as in mutants after 0h at 29°C (not shown). Hairy background was determined in the posterior part of the disc, where Hairy is not expressed. Background was subtracted before fitting (see below).

The **mitotic density profile** was quantified analogously, except that the projected PH3 image was binarised before analysis, i.e. values of pixels outside the disc were set to NaN, values of PH3-positive pixels were set to 1, and all others were set to 0. To avoid discrepancies between different stainings or imagings, a general procedure was developed. This procedure adjusts the binarisation threshold in such a way that the binarisation always leads to similarly sized PH3-positive spots, regardless of the original image (Fig. S1H,I). The procedure is iterative: at each step, the mean area of PH3-positive spots in the image is determined. If it is bigger than a fixed optimal value, the binarisation threshold is increased, until the mean area of spots is close to the optimal value.

The mitotic density profile was then converted into a **growth rate profile**. To find the conversion factor, we made use of the fact that the measured mean tissue growth rate in x-direction, $\bar{g}_x = \dot{L}_x / L_x$, must be equal to the integral of the PH3 profile times a conversion factor κ_x, $\kappa_x = \frac{\dot{L}_x / L_x}{\left(\int_0^{L_a} dx(PH3(x))\right) / L_x}$. Using this expression we find that the

value of κ_x is between 0.75 h^{-1} and 1 h^{-1} (Fig. S1J). Because the mitotic density is approximately equal to the duration of mitosis θ_M divided by the cell doubling time θ, $PH3 = \theta_M / \theta$, and because the growth rate is inversely proportional to the cell doubling time: $g = \ln 2 / \theta$, the conversion factor κ_x is also given by $\kappa_x = \ln 2 / (\theta_M (1 + \varepsilon))$. For a value of κ_x between 0.75 h^{-1} and 1 h^{-1}, and a measured $\varepsilon \approx 1$, this yields a duration of mitosis θ_M of between 21 and 28 minutes, which is in good agreement with experimental observations. For simplicity, from hereon we use $\kappa_x \approx 1$ h^{-1} to convert PH3 profiles into g_x profiles.

Finally, all profiles were shifted by (imageSize – furrowPosition) so that all profiles aligned with respect to their furrow positions (at x = 0). For the **mean profiles** shown, aligned profiles were normalised to their amplitude, and the mean profile shape with standard errors was determined for each time-point, for a group of time-points or for a group of discs as a function of relative position ($r = x / L_a$).

Quantification of intensity and mitotic density profiles in clones

For smo[3], mad[12], brk[M68] and mad[3] brk[M68] clones, larvae were heat-shocked at 60h after egg laying for 1 hour at 37°C. Larvae were dissected approximately three days later and fixed and stained as described above. Wherever possible, an internal control was chosen (e.g. measurements inside clones were compared to measurements outside clones but in the same discs) to minimize effects of stainings on the analysis.

Intensity and mitotic density profiles were quantified as described above, with the following difference. As above, the PH3 image was binarised, and the Hairy and PH3 values of pixels located outside the disc were set to NaN. In addition, a mask (a separate image) was created where values of pixels located inside clones were set to 1, and values of pixels outside clones were set to 0. There are therefore different pixel value combinations, notated as follows: NaN pixels are located outside of the disc, "$(\text{non}-\text{NaN}, \text{mask}=1)$" pixels are located inside clones, and "$(\text{non}-\text{NaN}, \text{mask}=0)$" pixels are located outside clones but inside the disc.

To analyse Hairy intensity and mitotic density **inside clones**, the intensity or mitotic density values were obtained as described above but using only the $(\text{non}-\text{NaN}, \text{mask}=1)$ pixels of each column of the chosen ROI. For those columns of the ROI for which there weren't any $(\text{non}-\text{NaN}, \text{mask}=1)$ pixels, for example if all the pixels of a column were located outside clones, the resultant values at that position were set to NaN. To analyse Hairy intensity and mitotic density **outside clones**, the same analysis was performed using the $(\text{non}-\text{NaN}, \text{mask}=0)$ pixels. Because clones never span a whole ROI, the sample size (number of clones contributing to the intensity or mitotic density values at a position) is different for each position (Fig. S1F).

Fitting of the theory to signaling intensity and mitotic density profiles

The amplitude of signaling profiles was determined directly for each profile as the maximum obtained from a smoothing spline fit. To determine the shape of profiles, the normalized profiles, $C(x)/C_{\max}=f_c(x)$, were fit by a custom fit function. This fit function has to fulfill the following requirements: it has a maximum, an exponential

tail, and it has to scale with L_a, so that its shape is constant when plotted over relative position. We constructed a fit function of the form: $C(x) = C_{\max} e^{-\int_0^x \lambda^{-1}(x)dx}$. Here, the inverse of the decay length, λ^{-1}, is a function of x. It is chosen such that it is zero at the position of the signaling peak, $x = x_c$, accounting for the maximum, but constant for $x > x_w$, accounting for the exponential tail (Fig. S1K). These properties are obeyed by the following function $f_c(x)$:

$$f_c(x) = \begin{cases} e^{\frac{(x-x_c-x_w)^3}{3\lambda_c x_w^2} - \frac{(x-x_c-x_w)}{\lambda_c} - \frac{2x_w}{3\lambda_c}} & \text{for } 0 \le x \le x_c + x_w \\ e^{-\frac{(x-x_c-x_w)}{\lambda_c} - \frac{2x_w}{3\lambda_c}} & \text{for } x > x_c + x_w \end{cases} \qquad \text{(supplementary equation 1).}$$

The function is piece-wise but continuous. At $x = x_c$, $f_c(x_c) = 1$ takes a maximal value so that $C(x_c) = C_{\max}$. Therefore, x_c is the position of the maximum of the concentration profile; x_w is the distance between this maximum and the start of the exponential tail of the profile; λ_c is the decay length of the exponential tail of the profile. To determine the scaled profile, $C(r)/C_{\max} = f_C(r)$, the parameters x_c, x_w and λ_c are divided by L_a, so that $r_c = x_c / L_a$, $r_w = x_w / L_a$ and $\phi_c = \lambda_c / L_a$. Scaling of the signaling profile implies that r_c, r_w and ϕ_c are constant for different L_a.

Using the fit function for C(x) we calculate the corresponding growth profile *g(x)* using equation 6, which is given by

$$g_x(x) = \begin{cases} g_{\max}\left(1 - \dfrac{(x - x_c - x_w)^2}{x_w^2}\right) e^{\frac{\gamma(x-x_c-x_w)^3}{3\lambda_c x_w^2} - \frac{\gamma(x-x_c-x_w)}{\lambda_c}} & \text{for } 0 \le x \le x_c + x_w \\ g_{\max} e^{-\frac{\gamma(x-x_c-x_w)}{\lambda_c}} & \text{for } x > x_c + x_w \end{cases}$$

$$\text{where } g_{\max} = \frac{v_S \gamma}{\lambda_c} e^{-\frac{2x_w\gamma}{3\lambda_c}} \qquad \text{(supplementary equation 2).}$$

In addition to the fit parameters of $f_c(x)$, there are two new fit parameters: g_{max}, which is approximately (but not exactly) equal to the amplitude, and γ (equation 2). The parameter g_{max} is constrained by the other parameters and the source velocity. Therefore the source velocity v_s can be calculated from the known values of fit parameters (supplementary equation 2 and Table S2). This value of the source velocity is thus obtained independently of the measured value. Supplementary equation 2 can be scaled with respect to L_a in the same way as described for supplementary equation 1 above. For the simultaneous fit of f_c and g to profiles obtained in wildtype, γ was a free fit parameter, and $\alpha = \dfrac{\ln 2}{\gamma(1+\varepsilon)}$ was calculated from this parameter with $\varepsilon = 1$ (Fig. S1A, Fig. 1E, equation 2).

With these equations, the fit to wildtype data performs very well ($R^2 = 0.96$; Fig. S1A), but slightly over-estimates the distance between the P-Mad and PH3 peaks. This may reflect the fact that the decision to undergo mitosis according to the temporal growth rule was made some time before cells became PH3-positive, during which time cells have moved towards the posterior. This means that the measured mitotic profile is slightly shifted to the posterior compared to the actual mitotic-decision-making profile. To account for a delay corresponding to a shift in the

proliferation profile, an additional parameter was introduced in the *g(x)* fit function to shift the profile along the r-axis: $x = x + x_{shift}$. Note that a shift along this axis in principle only affects the distance between the peaks – it has no direct effect on the value of α, because α is constrained by the decay of proliferation and concentration profiles, $\lambda_g = \lambda_c / \gamma$ (supplementary equations 1 and 2). However, as the shift allows for a better fit of the decay (compare Fig. 2F and Fig. S1A), the value of α obtained with this fit is probably more accurate than in a fit without shift. The delay τ between the decision to undergo mitosis and the appearance of PH3 can be estimated as $\tau \approx x_{shift} / v_S$, which in wildtype corresponds to approximately 1 hour.

For fits in the mutant conditions, α was set to 0.60 to test whether the data is consistent with the temporal model. This means that γ was fixed and that in these cases there were five fit parameters: r_c, r_w, r_{shift}, ϕ_c and g_{max}. After a first simultaneous fit of both signaling and growth profiles, *g(r)* was normalized to g_{max}. Then C/C_{max} and g/g_{max} profiles were fit simultaneously with only four parameters: r_c, r_w, r_{shift}, and ϕ_c. The parameters r_c, r_w and r_{shift} determine the position and distance between peaks, and the fit parameter ϕ_c together with the set γ determines the decay length of the proliferation rate anterior to the mitotic peak. When fitting the profiles for C765>Dpp, the equations were modified to include an offset, corresponding to the signaling level at the edge of the disc. This offset was measured and not fit.

Statistical analysis

For linear fits of the source velocity v_s and the anisotropy ε, the standard error σ_s was estimated from 67% confidence intervals returned by the fit programme (the curve

fitting tool in matlab). The goodness of the fit, R^2, for a given set of fit parameters is defined as 1 minus the residual sum of squares divided by the total sum of squares and thus indicates how well the given model can explain the variation in the data. For the simultaneous fits, an error σ_a for a fit parameter a of the fit function f was obtained from the dependence of the R^2 on the parameter a as follows:

$$\sigma_a = \pm \sqrt{\frac{-0.05 R_{opt}}{\frac{1}{2}\frac{d^2 R(a)}{da^2}\Big|_{a=a_{opt}}}} \qquad \text{(supplementary equation 3).}$$

Here $R(a)$ is the R^2 as a function of a and R_{opt} is the R^2 of the fit with the optimal fit parameter value a_{opt}. The factor 0.05 comes from the definition of a threshold of the R^2 below which the fit is no longer considered good. This threshold is defined as 95% of R_{opt}.

Theory

The contribution of the second mitotic wave to the increase of the posterior compartment width can be neglected.

This can be shown as follows: Posterior cells in the second mitotic wave reportedly divide only once, and not all cells divide. We estimate that the width of the posterior region, L_p, increases linearly due to this single cell division, in addition to an increase in width due to the movement of the source. The posterior width would thus be given by:

$$L_p = v_S t + v_P t \quad \text{(supplementary equation 4).}$$

The first term in supplementary equation 4 describes the increase in posterior width due to source movement (which is approximately linear, Fig. 1D), and the second term describes an increase in posterior width due to cell division in the posterior. This contribution is also approximately linear since posterior cells divide at most once. The expansion velocity due to growth in x-direction, v_p, is bounded by:

$$v_P < \frac{ap}{\theta} \qquad \text{(supplementary equation 5).}$$

Here a is the cell diameter ($a < 2\mu m$; as estimated from images), p is the percentage of cells that do divide in the second mitotic wave posterior to the furrow ($p < 1$, because not all cells divide, and those that do, divide only once) and θ is the cell cycle length ($\theta \geq 5h$; estimated from the shortest cell cycle length in the anterior). In addition, part of the growth will be absorbed in y-direction and will therefore not contribute to the increase of L_p; as a consequence, ap/θ constitutes an upper bound for v_p. The estimates for a, p and θ yield $v_P < 0.4\mu m/h$, which is small compared to $v_S \approx 3\mu m/h$. Therefore, the contribution of the second mitotic wave to the increase in the posterior width can be neglected.

Derivation of equation 3. From $C(x,t) = C_{\max}(t) f(x,t)$ (equation 1), it follows that $C_{cell}(t) = C_{\max}(t) f(x_{cell}(t),t)$. The relative time derivative is given by $\frac{\dot{C}_{cell}}{C_{cell}} = \frac{\dot{C}_{\max}}{C_{\max}} + \frac{\dot{f}}{f}$, which for a profile that scales can be written as:

$$\frac{\dot{C}_{cell}}{C_{cell}} = \frac{\dot{C}_{\max}}{C_{\max}} + \frac{1}{f}\frac{dr_{cell}}{dt}\frac{df}{dr_{cell}} \qquad \text{(supplementary equation 6),}$$

where, $r_{cell} = x_{cell} / L_a$. Therefore, $\frac{dr_{cell}}{dt} = \frac{\dot{x}_{cell} L_a - x_{cell} \dot{L}_a}{L_a^2}$, and $\frac{df}{dr_{cell}} = L_a \frac{df}{dx_{cell}}$. As a consequence,

$$\frac{\dot{C}_{cell}}{C_{cell}} = \frac{\dot{C}_{\max}}{C_{\max}} + \left(\dot{x}_{cell} - x_{cell} \frac{\dot{L}_a}{L_a} \right) \frac{\partial_x f}{f} \Big|_{x=x_{cell}} \qquad \text{(supplementary equation 7).}$$

With $v_{cell} = \dot{x}_{cell}$, and $\frac{\partial_x C}{C} = \frac{\partial_x f}{f}$, this yields equation 3. Note that supplementary equation 7 and equation 3 apply to both wing and eye discs.

Derivation of equation 5. From equation 4, it follows that $g_x = \partial_x v_g$, while equation 2 postulates that $g_x = \gamma \frac{\dot{C}_{cell}}{C_{cell}}$. Together with the expression for $\dot{C}_{cell} / C_{cell}$ given by supplementary equation 7, this results in

$$\partial_x v_g = \gamma \left(\frac{\dot{C}_{\max}}{C_{\max}} + \left(v_g - v_S - x_{cell} \frac{\dot{L}_a}{L_a} \right) \frac{\partial_x C}{C} \Big|_{x=x_{cell}} \right) \qquad \text{(supplementary equation 8).}$$

Here we used $v_{cell} = v_g - v_S$ (equation 4). Because $C_{\max}$ is proportional to L_a (Fig. S1C), it follows that, when $\dot{L}_a \approx 0$, $\dot{C}_{\max} \approx 0$, and supplementary equation 8 is reduced to equation 5. Note that supplementary equation 8 applies to both wing and eye discs, whereas the simplification of $\dot{L}_a \approx 0$ and equation 5 only apply in the eye disc.

Derivation of equation 6. We rewrite and integrate equation 5 in the following way:

$$\int_0^{v_g(x)} \frac{dv_g}{(v_g - v_S)} = \gamma \int_{C_{\max}}^{C(x)} \frac{dC}{C} \qquad \text{(supplementary equation 9).}$$

Here we make use of the fact that at for positions $x < x_c$, $v_g(x) = 0$, because at this positions, $\partial_x C$ is positive, resulting in negative $\dot{C}_{cell} / C_{cell}$ (see supplementary equation 7) and therefore no growth. Therefore, supplementary equation 9 yields:

$$v_g(x) = v_S\left(1 - \left(\frac{C(x)}{C_{\max}}\right)^{\gamma}\right) \qquad \text{(supplementary equation 10).}$$

Because $g_x = \partial_x v_g$ (equation 4), we can obtain an equation for $g_x(x)$ by deriving supplementary equation 10 with respect to x. This yields equation 6. Note that supplementary equation 10 and equation 6 only apply in the eye disc.

Data analysis of the timecourse after start of furrow movement (Fig. S1L-P and Supplementary Movie 1)

From the mean P-Mad (or Hairy) profiles quantified as a function of position (x) at different times (t), a **continuous concentration profile** $C(x,t)$ was reconstructed by interpolation (as described previously (Wartlick et al. 2011c) (Fig. S1N). From the quantified mitotic density profiles, a **continuous proliferation profile** $g_x(x,t)$ was obtained accordingly (Fig. S1O). Changes of cell positions in the growing tissue during time increments dt were then calculated based on equation 4:

$$x_{cell}(t+dt) = x_{cell}(t) + \left(\int_0^{x_{cell}} g_x(x,t)\, dx\right) dt - V_S dt \quad \text{(supplementary equation 11)}$$

to obtain time courses of cell positions. The second and third term correspond to the effects of proliferation and furrow movement on cell position, respectively: growth increases the distance between a cell and the furrow, whereas furrow movement

diminishes this distance (Fig. S1L). The resultant **cell positions over time**, $x_{cell}(t)$, are shown in Figure S1M. The **cellular concentration over time** was obtained from $C(x,t)$ with $C_{cell}(t) = C(x_{cell}(t),t)$ (Fig. S1N). The **cellular proliferation rate over time** was obtained from $g_x(x,t)$ with $g_{cell}(t) = (1+\varepsilon)\, g_x(x_{cell}(t),t)$, using the measured anisotropy ε≈1 (Fig. 1E; Figure S1O). The relationship between cellular concentration and cellular proliferation rates can then be explored. For the $g(\dot{C}/C)$ plot in Figure S1P, $\dot{C}_{cell}/C_{cell}$ was calculated from $C_{cell}(t)$ at different times and plotted against g_{cell} of these same times. The corresponding α=0.59 was obtained from the slope *s* of a linear fit with $\alpha = \frac{\ln 2}{s}$ (equation 2).

Supplementary Figure Legends

Figure S1. Supplementary data and methods. **A**, simultaneous fit to C/C_{max} and g without shift; the fit performs well but over-estimates the position between peaks, indicating that the proliferation profile may be shifted slightly; **B**, C_{max} of P-Mad and Hairy, as well as g_{max} over time; **C**, P-Mad and Hairy amplitude as a function of anterior width; arrows indicate trends (note that during development, the anterior width increases and then decreases (Fig. 1D); **D**, the growth rate g_c is the component of the growth rate that is due to changes in $\dot{C}_{\max}$, and was obtained from the fits of the proliferation data at different times of development (see Fig. 2E), using the fact that for $x \to L_a$, the value of $\dot{C}_{cell} / C_{cell} \to \dot{C}_{\max} / C_{\max}$ (equation 3) and therefore $g \to g_c$ (equation 2). Therefore, an approximate value of g_c can be obtained from the fitted $g(L_a)$. Values of $\dot{C}_{\max} / C_{\max}$ at the same developmental times were obtained from the experimental $C_{\max}$ data (Fig. S1B). Note that the relationship between g_c and $\dot{C}_{\max} / C_{\max}$ is linear, consistent with a temporal model (equation 2) and consistent with a value of α of 60% (blue line). The red box indicates data-points from developmental times where $\dot{C}_{\max} \approx 0$. **E**, anterior width over time in pent mutants (red) compared to wildtype; **F**, sample size for clonal analyses (Fig. 3 and 4) as a function of relative position; a "contributing disc" has a clone or tissue of the specified genotype that covers the position in question; **G**, hh^{ts2}/TM6B controls for the hh^{ts} experiment shown in Fig 4A; **H-I**, general method for detection of PH3-positive spots (**H**), generating binary images with spots of roughly equal area (red overlay on the original image in lower panel in **H**; see Supplementary Information); the mean area of spots per image is shown in **I**; **J**, calibration for conversion of mitotic density (PH3) into g_x (see Supplementary Information); **K**, the function λ^{-1} used to construct the fit function (see Supplementary Information). **L**, cell movement in the anterior region is affected by growth, which pushes cells away from the furrow, and furrow movement into the anterior, which reduces the distance between cells and the furrow. **M**, Cell trajectories can be calculated using the average growth profiles measured by PH3 staining and the measured furrow velocity (see supplementary material). Four sample cell trajectories are shown. **N**, **O**, continuous concentration and growth profiles as interpolated from the measured P-Mad and PH3 profiles. Cells that move in the tissue experience certain P-Mad concentrations (N) and exhibit certain cell growth rates (O), as illustrated by the four sample cell trajectories calculated in **M**. The growth rates shown here are actual growth rates, $g = (1+\varepsilon)\, g_x$ (equation 2), taking the measured anisotropy (Fig. 1E) into account. **P**, cell growth rates (based on O) and temporal changes in cell concentrations (based on N) are linearly related, with α=0.59. The four sample cells of S1M are shown in addition the behaviour of many more cells (small black dots) and their average (larger black circles).

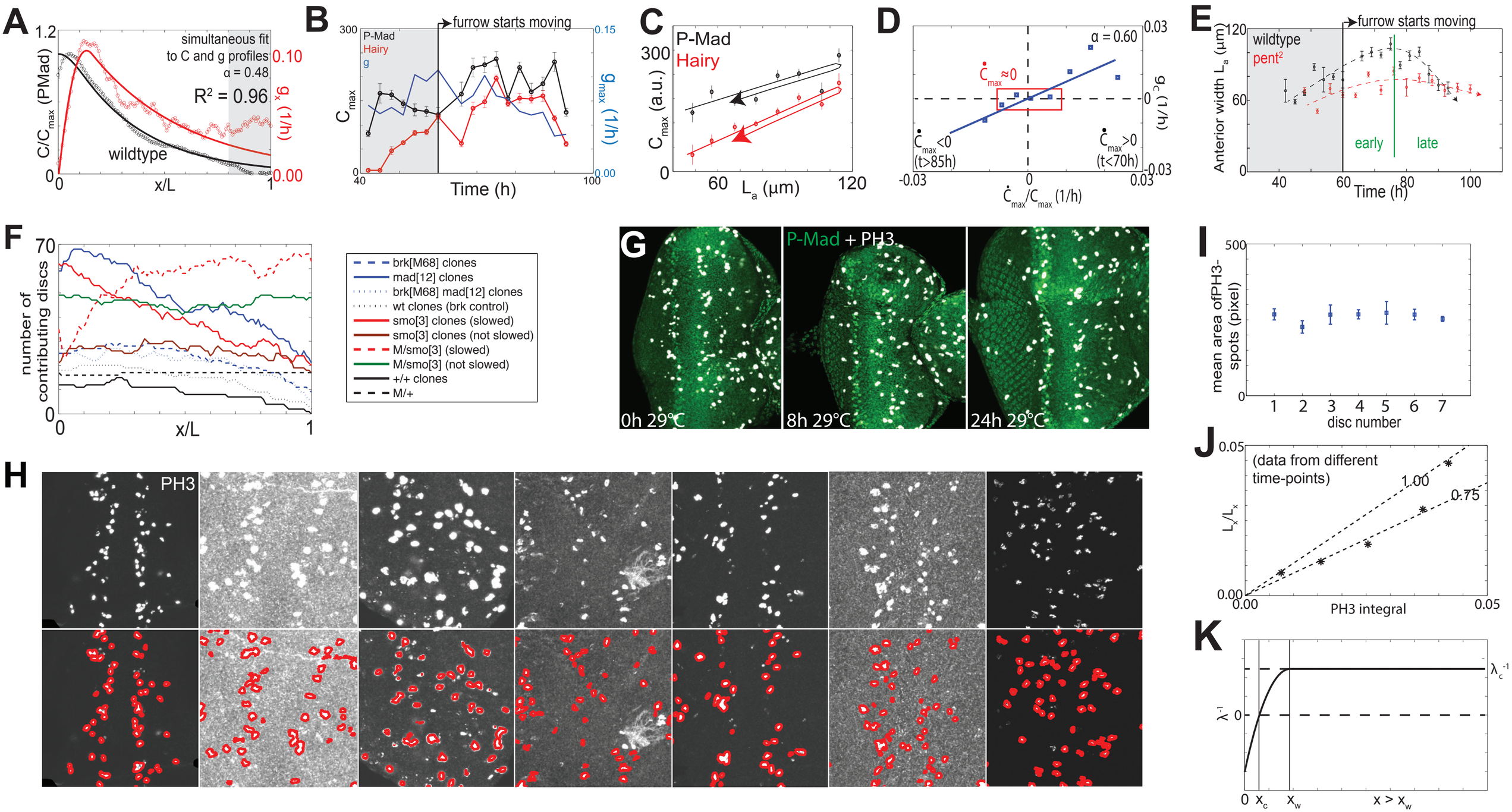

Supplementary Figure 1.

Supplementary Movie 1. This movie shows the data shown in Figure S1L-P in animated form, so is based on actual measured data. Top panel: each molecule is presented by a dot, and the gradient is represented by the number of dots as a function of position. The gradient scales with the size of the growing and shrinking tissue below it. In this tissue, four cells are marked: these cells move in the tissue over time according to the trajectories which were calculated in Fig. S1M. Bottom panel: As the cells move to different positions in the gradient, they experience different concentrations, which are tracked here over time (see also Fig. S1N). In the temporal model, cells divide when the concentration they perceive has increased by about 60%. These division events are marked by a star in all three panels. Note that 1) cell divisions are more likely to occur close to the furrow as cell concentrations increase markedly, and 2) cells which are positioned in the very anterior (for example the light blue cell and cells anterior to it), do not experience a large increase in concentration for much of development, and therefore do not divide often. Overall these effects lead to an accumulation of division events in front of the furrow (middle panel).

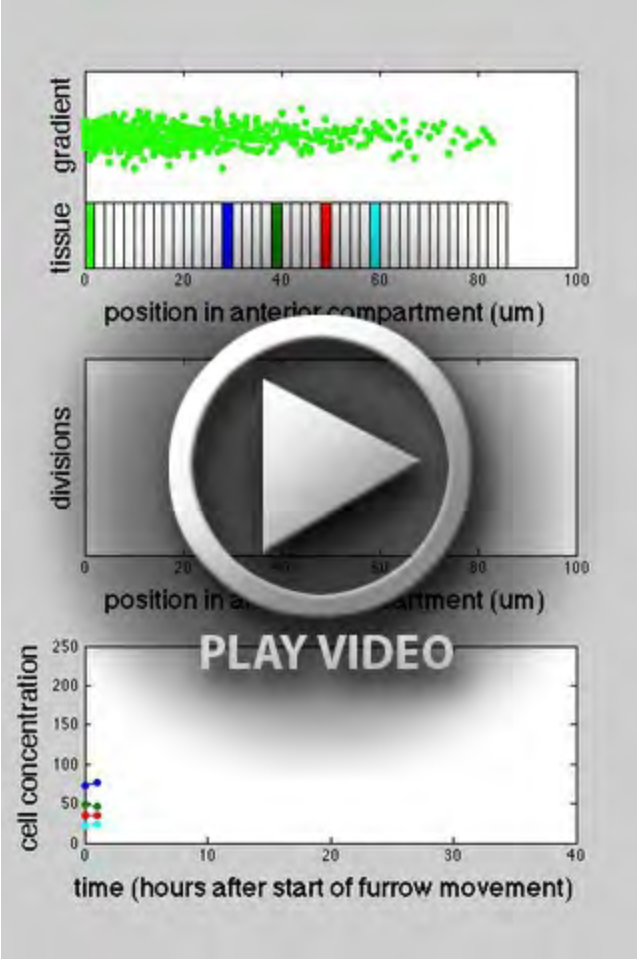

Supplementary Movie 1.

Table S1. Parameters used in the paper.

Parameters	Meaning	
L_a	anterior width	measured
L_p	posterior width	measured
$L_x = L_a + L_p$	total width in x-direction	measured
L_y	total width in y-direction	measured
g_x	growth rate in x-direction	extracted from fit to $L_x(t)$
g_y	growth rate in y-direction	extracted from fit to $L_y(t)$
$g = g_x + g_y$	growth rate	N/A
$\varepsilon = g_y / g_x$	anisotropy	extracted from fit to $\ln(L_y) = \varepsilon \ln(L_x)$
x	distance to the source	measured
x_{cell}	cell position with respect to the source	could be calculated with equation 4
$r = x / L_a$	relative distance to the source	calculated from x and L_a
t	time (after hatching)	measured
C	P-Mad or Hairy concentration	measured
$\dot{C}$	time derivative of C	could be calculated from a fit to C
$\partial_x C$	spatial derivative of C	measured
C_{max}	amplitude of the concentration profile	measured
λ_c	decay length of the exponential tail of the concentration profile C(x)	extracted from fit to $C(r)$ or from simultaneous fit to $C(r)/C_{max}$ and $g(r)$
$\phi_c = \lambda_c / L_a$	decay length of the exponential tail of the relative concentration profile C(r)	extracted from fit to $C(r)$ or from simultaneous fit to $C(r)/C_{max}$ and $g(r)$
$r_c = x_c / L_a$	relative position of the maximum of the concentration profile C(r)	extracted from fit to $C(r)$ or from simultaneous fit to $C(r)/C_{max}$ and $g(r)$
$r_g = x_g / L_a$	relative position of the mitotic peak	numerical estimation based on fit to $g(r)$ or simultaneous fit to $C(r)/C_{max}$ and $g(r)$
$\gamma = \frac{\ln 2}{\alpha(1+\varepsilon)}$	parameter of the temporal growth model, incorporating growth anisotropy	extracted from simultaneous fit to $C(r)/C_{max}$ and $g(r)$
α	percentage by which signaling levels increase during one cell cycle	extracted from γ
$\lambda_g = \lambda_c / \gamma$	decay length of the exponential tail of the proliferation profile g(x)	extracted from simultaneous fit to $C(r)/C_{max}$ and $g(r)$
$\phi_g = \lambda_g / L_a$	decay length of the exponential tail of the proliferation profile g(r)	extracted from simultaneous fit to $C(r)/C_{max}$ and $g(r)$
$v_S \approx \dot{L}_p / L_p$	source velocity	extracted from fit to $L_p(t)$ or from simultaneous fit to $C(r)/C_{max}$ and $g(r)$
v_g	velocity field due to growth	could be calculated with equation 4 or with supplementary equation 10
$v_{cell} = v_g - v_s$	cell velocity	could be calculated from v_S and v_g
$g_{\max} = v_s \gamma / (\phi_c L_a)$	amplitude of proliferation profile	measured (based on PH3 profile) or extracted from simultaneous fit to $C(r)/C_{max}$ and $g(r)$
r_{shift}	shift between the mitotic decision making profile and the PH3 profile	extracted from simultaneous fit to $C(r)/C_{max}$ and $g(r)$
$\tau = r_{shift} L_a / v_s$	delay interval between decision to undergo mitosis and appearance of PH3	calculated from simultaneous fit parameters r_{shift} and v_s and the measured L_a

Table S2. Parameter values.

	wildtype	**pent^{2}**	**C765>Dpp**	**mad^{12}**	**brk^{M68}**	**mad^{12} brk^{M68}**
R^2	0.95	0.95	0.89	0.91	0.91	0.87
r_c	0.09±0.03	0.09±0.02	0.15±0.02	0.08±0.01	0.16±0.02	0.08±0.01
r_w	0.13±0.06	0.09±0.05	0.15±0.09	0.06±0.04	0.18±0.06	0.04±0.03
r_{shift}	0.08±0.04	0.10±0.02	0.10±0.03	0.08±0.02	0.13±0.03	0.05±0.01
ϕ_c	0.23±0.06	0.18±0.05	0.16±0.05 (fit with offset=0.47)	0.18±0.04	0.32±0.07	0.25±0.05
α (set value)	N/A	0.60	0.60	0.60	0.60	0.60
α_{Hairy} (fit value)	0.71±0.25	0.87±0.31	0.59±0.64	0.69±0.22	0.50±0.16	0.62±0.17
α_{PMad} (fit value)	0.57±0.19	0.75±0.26	0.52±0.43	N/A	N/A	N/A
g_{max}	0.07	0.10	0.12	0.10	0.09	0.16
L_a	(84±16) μm	(60±12) μm	(75±15) μm	(76±13) μm	(49±7) μm	(82±11) μm
ε	1.09±0.03	1.04±0.04	1.0	1.0	1.0	1.0
v_s (measured)	(3.1±0.3) μm/h	(2.1±0.2) μm/h	N/A	N/A	N/A	N/A
v_s (calculated)	2.9 μm/h	2.2 μm/h	3.6 μm/h	2.8 μm/h	3.1 μm/h	6.1 μm/h
delay (calculated)	(2.2±0.1) h	(2.7±0.2) h	(2.3±0.2) h	(2.2±0.2) h	(2.1±0.1) h	(0.6±0.6) h

Table S2. Parameter values. Parameters for simultaneous fits to *C(r)* and *g(r)* profiles shown in Fig. 2F,I,L, Fig. 4D,H,L, based on equation 6 (see Supplementary Information for fit function), as well as other, measured parameters. For wildtype, pent^{2} and C765>Dpp fits both P-Mad and Hairy profiles were used; for *mad^{12}*, *brk^{M68}* and *mad^{12} brk^{M68}*, Hairy profiles were used. White shading: value given by the simultaneous fit; purple shading: set values; gray shading: measured values; dark gray shading: values calculated from fit parameters and/or measured values. For the fits shown in Fig. 2I,L, Fig. 4D,H,L, the value of α was set to 0.60 (set value). The value of α obtained from an unconstrained fit is also given in the table (fit value). Errors for simultaneous fit parameters were calculated as described in the Supplementary Information.